Journal of Medicinal Chemistry

pubs.acs.org/jmc Article

Development of Novel ^{18}F-PET Agents for Tumor Hypoxia Imaging

Li Wang, Hui Wang, Kun Shen, Hyejin Park, Tao Zhang, Xuedan Wu, Mei Hu, Hong Yuan, Yue Chen, Zhanhong Wu,* Qiu Wang,* and Zibo Li

Cite This: *J. Med. Chem.* 2021, 64, 5593−5602 Read Online

ACCESS | Metrics & More | Article Recommendations | Supporting Information

ABSTRACT: Tumor hypoxia is a major factor responsible for tumor progression, metastasis, invasion, and treatment resistance, leading to low local tumor control and recurrence after radiotherapy in cancers. Here, ^{18}F-positron emission tomography (PET) probes are developed for visualizing viable hypoxic cells in biopsies. Pimonidazole derivatives and nitroimidazole-based agents bearing sulfonyl linkers were evaluated. A small-animal PET study showed that the tumor uptake of [^{18}F]-**23** [poly(ethylene glycols) (PEG)−sulfonyl linker] of 3.36 ± 0.29%ID/g was significantly higher (P < 0.01) than that of [^{18}F]-**20** (piperazine-linker tracer, 2.55 ± 0.49%ID/g) at 2 h postinjection in UPPL tumors. The tumor-to-muscle uptake ratio of [^{18}F]-**23** (2.46 ± 0.48 at 2 h pi) was well improved compared with that of [^{18}F]-FMISO (1.25 ± 0.14 at 2 h pi). A comparable distribution pattern was observed between *ex vivo* autoradiography of [^{18}F]-**23** and pimonidazole staining of the neighboring slice, indicating that [^{18}F]-**23** is a promising PET agent for hypoxia imaging.

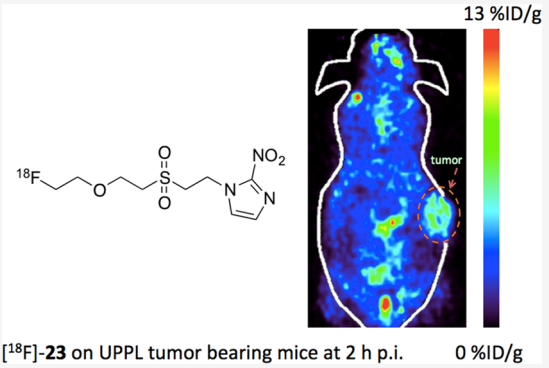

INTRODUCTION

Cancer is the second leading cause of death globally, claiming over 9.5 million lives worldwide. In addition to conventional cancer therapies, such as surgery, chemotherapy, and radiotherapy, considerable effort has been devoted to the development of new anticancer agents, including small molecular compounds,[1,2] metal complexes,[3−5] and antibody therapy.[6,7] Consequently, providing suitable therapy to patients becomes especially important. Hypoxia, a condition that leads to low oxygen levels in tissues, plays an important role in promoting tumor progression, angiogenesis, and resistance to radiotherapy and chemotherapy.[8,9]

Hypoxia is a common phenomenon in solid malignant tumors, characterized by higher resistance to therapy, and an indicator of poor prognosis.[10] For example, the degree of hypoxia in prostate cancer was shown to be a strong predictor for treatment failure in patients with localized prostate cancer after brachytherapy.[11] Various methods have been developed for hypoxia detection, such as Eppendorf O_2 polarographic needle electrodes,[12] exogenous markers,[13] immunohistochemical (IHC) analysis of endogenous tumor hypoxia markers,[14] magnetic resonance imaging,[15] and hypoxia positron emission tomography (PET).[16] As a noninvasive, quantitative, and highly sensitive imaging method,[17] PET has been used to delineate the behavior of tumor hypoxia during therapy, thus offering improved treatment plan and prognosis for patients.[18]

A number of hypoxia PET probes have been developed in the last three decades, including F-18-, Ga-68-, Cu-64-, and I-123-labeled hypoxia PET agents.[19−21] Among them, the F-18-labeled nitroimidazole derivatives, such as ^{18}F-FMISO and ^{18}F-FAZA,[22,23] have been applied in basic and clinical research because of their suitable half-life and contrast (Figure 1). The

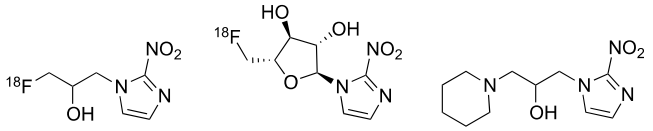

Figure 1. Nitroimidazole-based hypoxia PET tracers and staining agent pimonidazole.

nitroimidazole analogues have been widely used as a motif targeting hypoxic environments due to the hypoxia-selective mechanism of action. Normally, the nitro groups in nitroimidazole compounds are enzymatically reduced in all tissues. The intermediates are immediately oxidized back to the starting material in the presence of normal levels of oxygen. In hypoxic tissues, however, these electrophilic intermediates react further and form adducts with DNA and proteins.

Despite the advances in nitroimidazole-based probes, there remains a great need to develop new hypoxia PET agents.

Received: November 25, 2020
Published: April 26, 2021

Pimonidazole is widely used in hypoxia staining due to its relatively short plasma half-life and low background. Thus, PET agents derived from the pimonidazole skeleton may seamlessly integrate PET images with current pimonidazole-based staining to provide favorable tumor-to-reference tissue contrast.[24] Unfortunately, investigations of pimonidazole-based PET agents have been limited due to challenges in efficiently introducing ^{18}F into the parent pimonidazole compound. Herein, we report our initial attempts to develop PET agents based on the pimonidazole core structure. Moreover, neutral poly(ethylene glycol) (PEG)−sulfonyl linkers were introduced between ^{18}F and the imidazole motif, which were then evaluated *in vivo* to study the effects of side chains on nitroimidazole-based hypoxia probes. The goal of this study was to design and evaluate novel hypoxia PET agents, focusing on the modifications of the side chains.

RESULTS AND DISCUSSION

Chemical and Radiochemical Syntheses. Our initial approach focused on synthesizing pimonidazole-based PET tracers by a *N*-iodosuccinimide (NIS)-mediated cyclization, a novel radiofluorination method that we have recently reported.[25] The synthetic attempts are outlined in Scheme 1. We started with the fluorination of compound **1**, a readily accessible starting material. Yet, fluorinated product **2** was obtained in an extremely low yield, potentially due to the steric hindrance of the methyl group. Alternatively, compound **3** was synthesized and subjected to the NIS-mediated fluorination reaction to afford standard **4** smoothly (34% yield; details in the Supporting Information). However, the radiofluorination of **3** failed to form [^{18}F]-**4**, possibly owing to the presence of a free hydroxyl group. While a 2-tetrahydropyranyl (THP)-protected precursor **5** successfully led to the formation of [^{18}F]-**6**, the deprotection of the THP group of [^{18}F]-**6** with hydrochloric acid failed to yield [^{18}F]-**4**. Finally, in an attempt to introduce ^{18}F into the piperidine ring using compound **7**, the radiolabeled [^{18}F]-**8** was not detected, but rather an undesired elimination reaction was found to be a dominant pathway.

Compounds with Diamine Linkers. In light of these unexpected problems, we modified our probe design and focused on labeling the imidazole with diamine-linked poly(ethylene glycols) (PEG) (Scheme 2). A series of diamine-linked polyethylene glycol hypoxia tracers were then synthesized. Starting from di-tosylate-PEG1 (**9**) and di-tosylate-PEG2 (**12**), respectively, the reactions with ^{18}F-TBAF at 110 °C,[26] followed by purification with semi-high-pressure liquid chromatography (HPLC) gave the intermediates [^{18}F]-**10** and [^{18}F]-**13**. Substitution reactions of [^{18}F]-**10** and [^{18}F]-**13** with diamines produced [^{18}F]-**11**, [^{18}F]-**14**, or [^{18}F]-**15**, which then reacted with 1-(2,3-epoxypropyl)-2-nitroimidazole to provide the final products [^{18}F]-**20**, [^{18}F]-**21**, and [^{18}F]-**22** in moderate radiochemical yield (RCY).

Compounds with Sulfonyl Linkers. It has been shown that the overall charge and electronic properties of molecules can significantly alter the compounds' biodistribution potency.[27] The diamine linkers in **20**−**22** are generally considered to be positively charged candidates, as they are likely to be protonated in aqueous media. In contrast, sulfone moieties (−SO_2R) have been widely used in medicinal chemistry as a neutral linker.[28] The sulfone group can act as a less polar variant of diphosphate and as a pro-drug by releasing sulfonic acid after hydrolysis to mimic some bioactive

Scheme 1. Initial Trials of Pimonidazole-Based PET Tracer Synthesis[a]

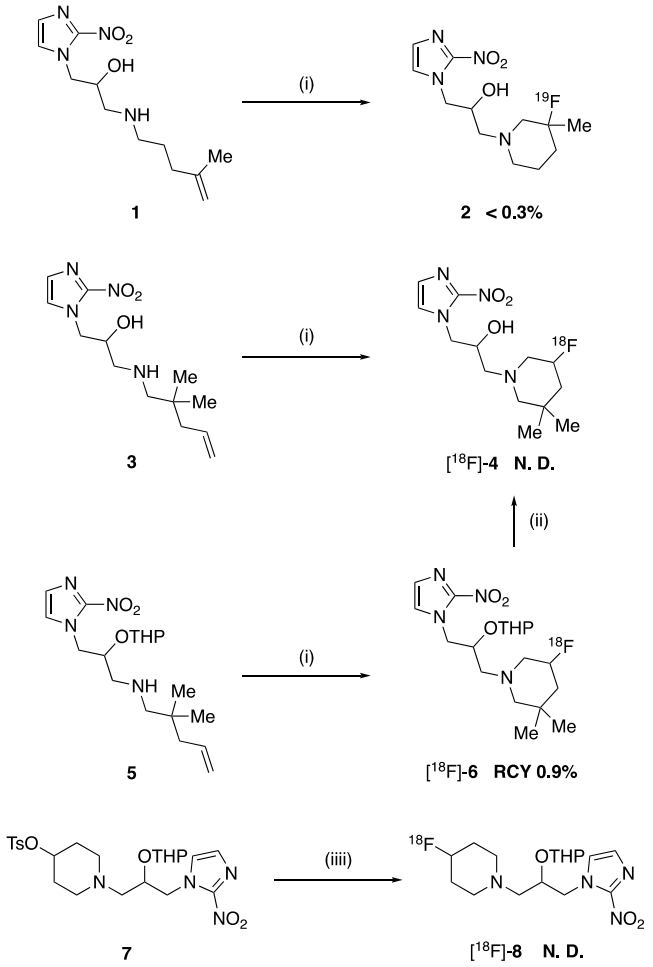

[a](i) NIS, room-temperature (RT), 10 min, followed by incubation with [^{19}F]/[^{18}F]-tetra-*n*-butylammonium fluoride (TBAF) at RT for 10 min; (ii) 1 N HCl, 80 °C, and 5 min; and (iii) [^{18}F]-TBAF, 110 °C, and 10 min.

agents including antibiotic analogues.[29] The Michael addition between vinyl sulfone and amine or thiol groups in biomolecules has demonstrated its great potential in developing imaging tracers or treatment agents.[30−32] We therefore designed compounds **23**−**25** bearing a sulfone linker as neutrally charged candidates. In brief, [^{18}F]-**17** and [^{18}F]-**19** were synthesized from **16** and **18** through the S_N2 reaction with [^{18}F]-TBAF. The reactions of [^{18}F]-**17** with 2-nitroimidazole were performed at pH 8.5 in a borate buffer and DMSO mixture, which led to [^{18}F]-**23** with a separation RCY of 58.7%. [^{18}F]-**24** was synthesized from [^{18}F]-**17** using 4-nitroimidazole. [^{18}F]-**25** was analogous to [^{18}F]-**23** but with an increased length of the PEG chain. RCY results of the above PET tracers are summarized in Table 1. Generally, the labeling yields of sulfone-based hypoxia tracers (53.1−66.8%) were higher than those of piperazine-based hypoxia tracers (22.8−29.0%). The identities of these agents ([^{18}F]-**20**−[^{18}F]-**25**) were confirmed by co-injection with the nonradiolabeled standards ([^{19}F]-**20**−[^{19}F]-**25**) (HPLC spectra presented in the Supporting Information).

We also attempted to develop a more concise synthesis of [^{18}F]-**23** through precursor **26** (Scheme 3). Although the

https://doi.org/10.1021/acs.jmedchem.0c01962
J. Med. Chem. 2021, 64, 5593−5602

Scheme 2. Synthesis of PET Agents [^{18}F]-20 to [^{18}F]-25[a]

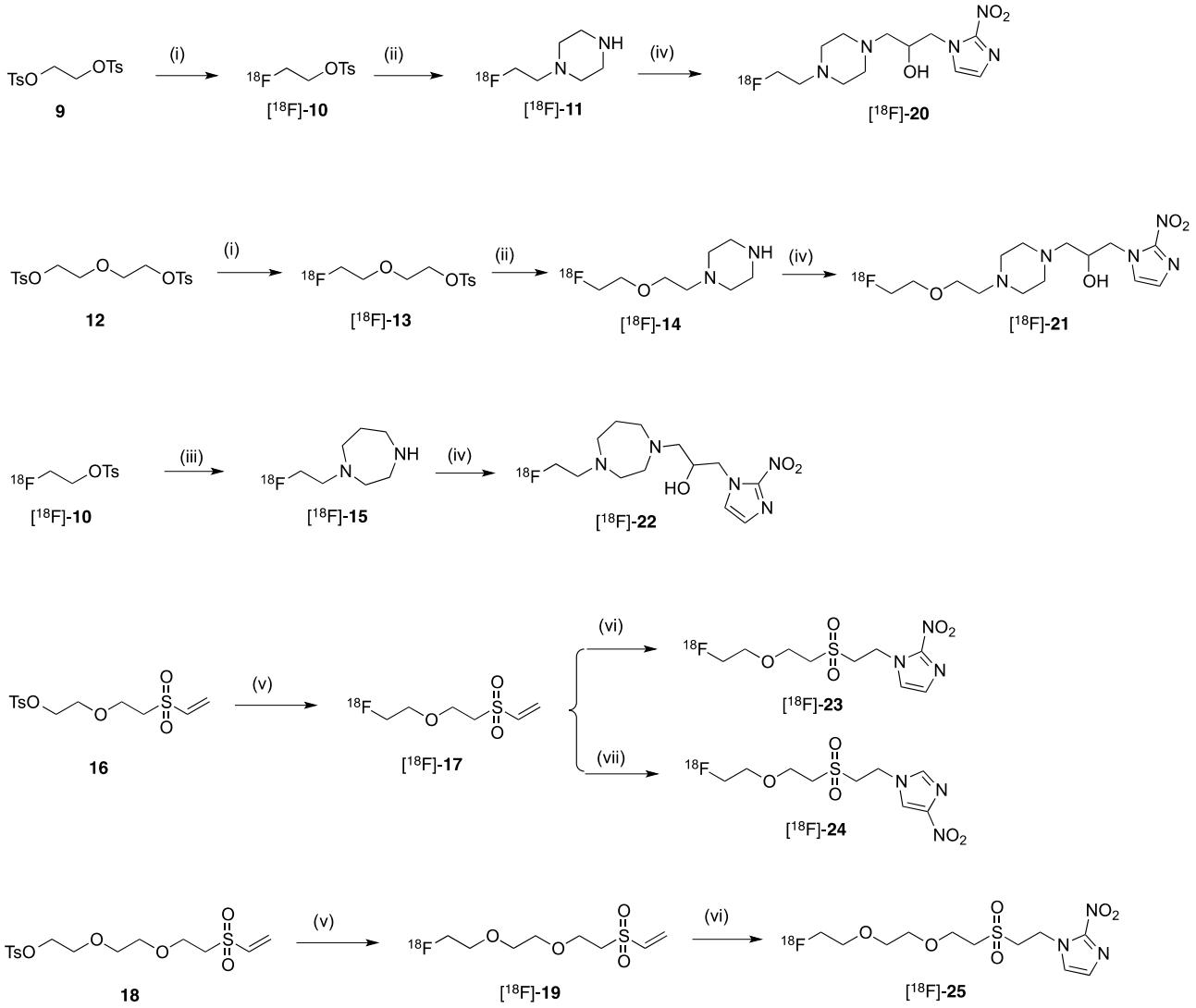

[a](i) [^{18}F]-TBAF, 110 °C, and 15 min; (ii) piperazine, 110 °C, and 10 min; (iii) homopiperazine, 110 °C, and 10 min; (iv) potassium carbonate, 1-(2,3-epoxypropyl)-2-nitroimidazole, 90 °C, and 20 min; (v) [^{18}F]-TBAF, 110 °C, and 20 min; (vi) 2-nitroimidazole, borate buffer, pH 8.5, and dimethyl sulfoxide (DMSO); and (vii) 4-nitroimidazole, borate buffer, pH 8.5, and DMSO.

Table 1. Radiosynthetic Yields for [^{18}F]-20, [^{18}F]-21, [^{18}F]-22, [^{18}F]-23, [^{18}F]-24, and [^{18}F]-25

compound	[^{18}F]-20	[^{18}F]-21	[^{18}F]-22	[^{18}F]-23	[^{18}F]-24	[^{18}F]-25
RCY[a]	29.0%	22.8%	28.8%	58.7% (1.4%[b])	66.8%	53.1%

[a]Final step yield based on the HPLC separation with the methods shown in Scheme 2. [b]Final step yield based on the HPLC separation with an alternate protocol shown in Scheme 3.

Scheme 3. Alternative Synthetic Protocol of [^{18}F]-23[a]

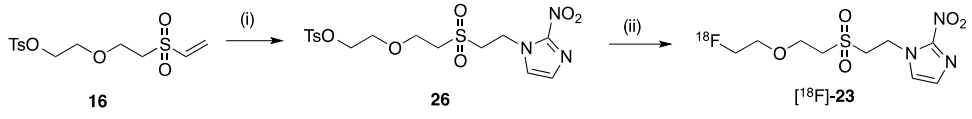

[a](i) 2-nitroimidazole, borate buffer, pH 8.5, and DMSO; (ii) [^{18}F]-TBAF, 110 °C, acetonitrile, and 20 min.

process was greatly simplified, one-step radiofluorination of **26** only led to [^{18}F]-**23** in 1.4% RCY. Further increase in the reaction temperature or switching to K^{18}F/Kriptofix failed to improve the labeling yield due to increased precursor decomposition. We therefore used the synthetic method shown in Scheme 2 to prepare [^{18}F]-**23** for its evaluation in the tumor imaging profile.

Small-Animal PET Imaging. Screening of PET agents [^{18}F]-**20**–[^{18}F]-**23** was first performed on nude mice bearing FaDu tumors (a well-established model for hypoxia imag-

https://doi.org/10.1021/acs.jmedchem.0c01962
J. Med. Chem. 2021, 64, 5593−5602

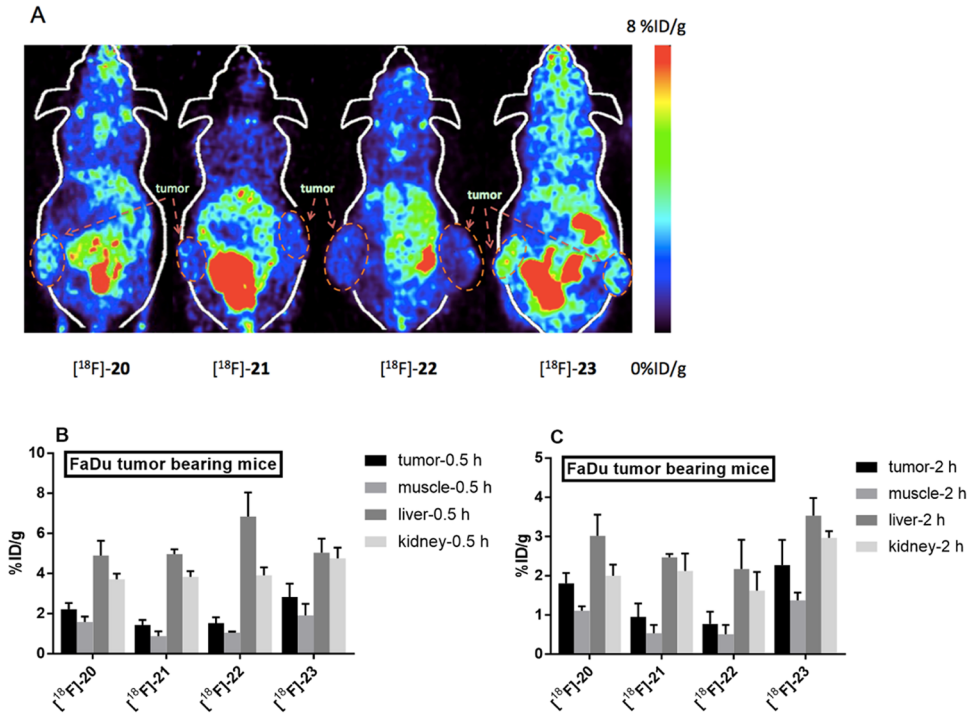

Figure 2. Evaluation of [^{18}F]-**20** to [^{18}F]-**23** in tumor-bearing mice. (A) PET image of FaDu tumor-bearing mice at 2 h postinjection. (B) Major organ and tumor uptakes of [^{18}F]-**20**, [^{18}F]-**21**, [^{18}F]-**22**, and [^{18}F]-**23** in nude mice bearing FaDu tumors at 0.5 h postinjection (three mice per group). (C) Major organ and tumor uptakes of [^{18}F]-**20**, [^{18}F]-**21**, [^{18}F]-**22**, and [^{18}F]-**23** in nude mice bearing FaDu tumors at 2 h postinjection (three mice per group).

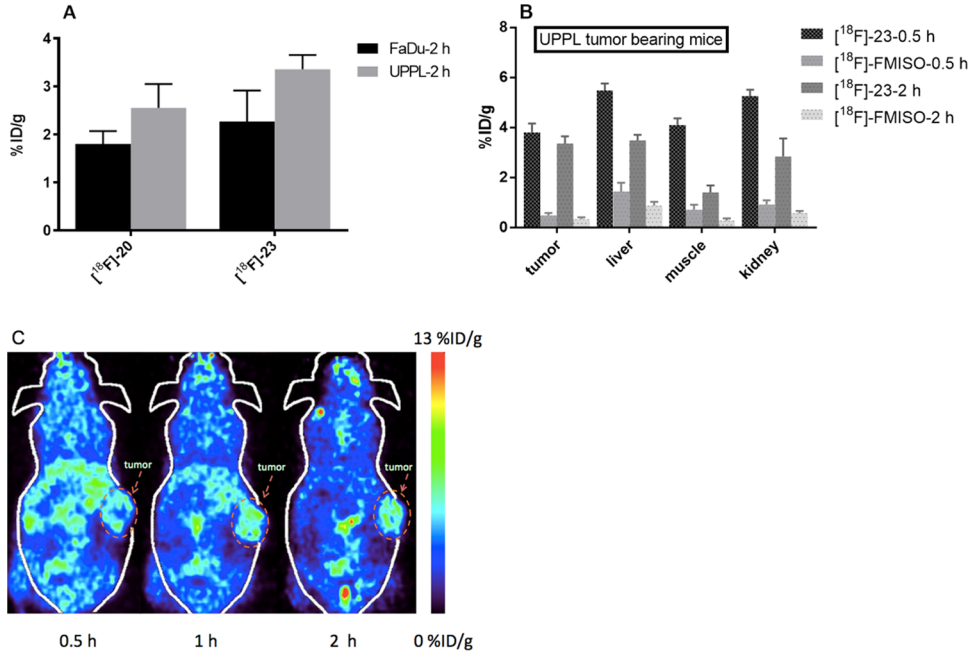

Figure 3. (A) Tumor uptake of [^{18}F]-**20** and [^{18}F]-**23** in nude mice bearing the FaDu tumor or black mice bearing the UPPL tumor at 2 h postinjection (three mice per group). (B) Major organ uptakes of [^{18}F]-**23** and [^{18}F]-FMISO in black mice bearing the UPPL tumor at 2 h postinjection (three mice per group). (C) Representative PET images of a UPPL tumor-bearing mouse at 30, 60, and 120 min postinjection of [^{18}F]-**23**.

ing).[33] PET scanning was performed at 0.5 and 2 h post-tracer injection. Representative images of [^{18}F]-**20** to [^{18}F]-**23** on FaDu tumor-bearing mice are shown in Figure 2A. The tumor uptakes of [^{18}F]-**20** to [^{18}F]-**23**, which were presented as mean ± standard deviation (SD), were 2.21 ± 0.31, 1.43 ± 0.25, 1.52 ± 0.30, and 2.82 ± 0.66%ID/g at 0.5 h pi and 1.80 ± 0.27, 0.95 ± 0.34, 0.77 ± 0.31, and 2.27 ± 0.64%ID/g at 2 h pi, respectively. Compared with [^{18}F]-**20** (tumor uptake value of 2.21 ± 0.31%ID/g and tumor-to-muscle ratio of 1.37 ± 0.18 at 2 h pi), the lower tumor uptake of [^{18}F]-**21** (1.43 ± 0.25%ID/g) and low tumor-to-muscle ratio of [^{18}F]-**22** (0.74 ± 0.16) did not warrant their further investigation as hypoxia imaging

https://doi.org/10.1021/acs.jmedchem.0c01962
J. Med. Chem. 2021, 64, 5593−5602

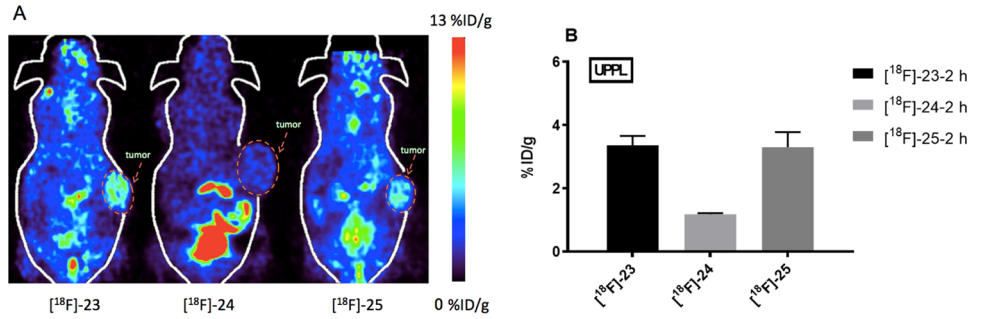

Figure 4. (A) PET image on UPPL tumor-bearing mice at 2 h postinjection. (B) Tumor uptake quantification of [^{18}F]-**23**, [^{18}F]-**24**, and [^{18}F]-**25** in black mice bearing UPPL tumors at 2 h postinjection (three mice per group).

agents. Replacing the piperazine motif with homopiperazine ([^{18}F]-**22**) also led to decreased tumor uptake *in vivo*. [^{18}F]-**23**, the agent with a sulfone linker, demonstrated the highest tumor uptake among these four agents. These preliminary studies suggested that [^{18}F]-**20** and [^{18}F]-**23** are promising hypoxia tracers, although a relatively high background was still observed. This also indicated that the neutral PEG−sulfonyl linker may be beneficial in the biodistribution of the tracer.

In addition to the FaDu tumor, hypoxia is also common in the microenvironment of various solid tumors, including bladder cancer. Recent studies have shown that hypoxic bladder cancer cells remodel the tumor microenvironment to facilitate tumor growth,[34] and treatments targeting hypoxic cells have obtained promising results in bladder cancer therapy.[35] A hypoxia imaging agent would work as a companion diagnostic and prognosis biomarker in the study of hypoxic bladder cancers. Therefore, we evaluated our newly developed agents in bladder cancers using UPPL tumors (luminal-like bladder cancer cell line (named UPPL)).[36]

As shown in Figure 3A, [^{18}F]-**23** demonstrated higher uptake (3.36 ± 0.29%ID/g at 2 h pi) than [^{18}F]-**20** (2.55 ± 0.50%ID/g at 2 h pi) in the UPPL tumors. Both agents showed increased uptake in the UPPL tumor ($P < 0.05$) compared with that of the FaDu tumor ($P > 0.05$). The tumor uptakes of [^{18}F]-**23** in the UPPL model are 3.80 ± 0.35, 4.02 ± 0.48, and 3.36 ± 0.29%ID/g at 30, 60, and 120 min pi, respectively. The comparison with a well-established hypoxia agent [^{18}F]-FMISO was also performed in the UPPL model (Figure S36). [^{18}F]-**23** demonstrated higher tumor uptake but comparable contrast compared with [^{18}F]-FMISO at 0.5 h pi ($P < 0.01$). The contrast of [^{18}F]-**23** became significantly higher than [^{18}F]-FMISO at 2 h pi ($P < 0.01$, Figure 3B). The tumor/muscle uptake ratios of [^{18}F]-**23** are 0.93 ± 0.08 and 2.46 ± 0.48 at 0.5 and 2 h pi, respectively, compared with 0.84 ± 0.20 and 1.25 ± 0.14 at 0.5 and 2 h pi, respectively, for [^{18}F]-FMISO. The representative images of tracer [^{18}F]-**23** in UPPL tumor-bearing mice show that the contrast was improved at the 2 h time point post the tracer injection compared to the images at 0.5 and 1 h pi (Figure 3C).

In addition to [^{18}F]-**23**, [^{18}F]-**24** and [^{18}F]-**25** were also evaluated in mice bearing UPPL tumors, and the results are summarized in Figure 4A. The replacement of 2-nitroimidazole ([^{18}F]-**23**, 3.36 ± 0.29%ID/g, $n = 3$/group) with 4-nitroimidazole (Figure 4B, [^{18}F]-**24**) resulted in a significant decrease in tumor uptake (1.18 ± 0.04%ID/g, $n = 3$/group, $P < 0.01$). Extending the PEG linker led to comparable tumor uptake ([^{18}F]-**25**, 3.30 ± 0.47%ID/g, $n = 3$/group, $P > 0.05$). Overall, the PEG1−sulfonyl-2-nitro-imidazole tracer [^{18}F]-**23** was the most promising candidate among the six PET tracers with various linkers. We observed bone uptake when the mice were scanned ([^{18}F]-**25**, Figure S37) at 4 h postinjection, suggesting defluorination of this kind of tracer at a later time point.

***In Vitro* and *In Vivo* Stability.** The *in vitro* and *in vivo* stability of [^{18}F]-**23** was evaluated (Figures S29−S34). As shown in Figures S29−S31, [^{18}F]-**23** was stable in plasma, with no apparent decomposition after 2 h incubation. After injecting into an animal, the agent decomposed quickly as found when the blood was analyzed (Figures S32−S34). Only 41.76% of [^{18}F]-**23** remained unchanged at 30 min postinjection, which was further decreased to the baseline level at 1 and 2 h pi. This may be caused by the fast clearance of the agent from blood and the complexity of the *in vivo* enzymatic environment. In one aspect, the hypoxia agents need to be retained in tumor cells due to the hypoxic environment; yet, the agent also needs to be cleared from normal tissues to improve contrast. Although we observed improved contrast of [^{18}F]-**23** in hypoxia tumors, detailed mechanism studies are still needed in the future to better design the agent.

Autoradiography. To investigate the distribution of our PET agent within tumors, UPPL tumors were collected, followed by *ex vivo* autoradiography and IHC of pimonidazole staining using neighboring slices (Figure 5). Pimonidazole is a

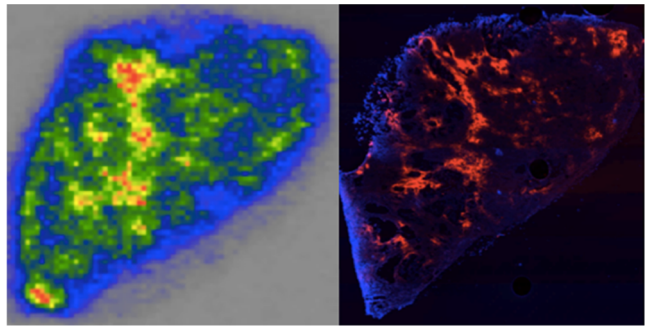

Figure 5. Autoradiography (left) and pimonidazole staining (right) of tumor tissues with [^{18}F]-**23**.

hypoxia marker widely applied in the study of tumor hypoxia and cell proliferation in tumor, so comparison of pimonidazole IHC and *ex vivo* autoradiography would confirm the tracer distribution.[37−39] As shown in Figure 5, the pimonidazole-positive hypoxia regions were observed on staining (right image). Similarly, in the neighboring slice, [^{18}F]-**23** was also heterogeneously distributed within the tumor (left image). The intratumor distribution of [^{18}F]-**23** on *ex vivo* autoradiography was visually similar to the histopathological distribution of

https://doi.org/10.1021/acs.jmedchem.0c01962
J. Med. Chem. 2021, 64, 5593−5602

pimonidazole. The distribution of [^{18}F]-**23** shown in the lower area of the tumor, found on autoradiography but not on pimonidazole staining, was most likely caused by either a cutting and section mounting error or using neighboring slices instead of the same slice. Nonetheless, it is notable that the staining experiment provided promising preliminary results. Additional study is needed in the future to further confirm the hypoxia specificity of the [^{18}F]-**23**.

CONCLUSIONS

Six potential hypoxia agents were synthesized and evaluated in our studies. PEG−Sulfonyl-based hypoxia agent [^{18}F]-**23** has demonstrated prominent uptake (3.36 ± 0.29%ID/g at 2 h pi in the UPPL tumor model) with a relatively low muscle uptake. Autoradiography and pimonidazole staining of neighboring slides showed a similar distribution pattern, indicating the promising potential of [^{18}F]-**23** for imaging hypoxia tumor tissue. Our findings warrant the use of a neutral sulfonyl group as a suitable scaffold to further expand the library of novel PET hypoxia tracers and/or hypoxia treatment agents.

EXPERIMENTAL SECTION

General. All chemicals were used as received from their manufacturer (Sigma-Aldrich, Fisher Scientific, and Alfa Aesar) unless otherwise noted. Nuclear magnetic resonance spectra were obtained on a Bruker AVANCE 400 MHz spectrometer. HPLC was carried out with either a Shimadzu Nexera XR LC-20AD equipped with a PDA detector or a Shimadzu LC-20AT Prominence equipped with a UV detector. The purity of all final compounds was ≥95% as determined by HPLC analysis.

Synthesis of Compounds 1, 3−7. *1-((2,2-Dimethylpent-4-en-1-yl)amino)-3-(2-nitro-1H-imidazol-1-yl)propan-2-ol (**1**).* A 25 mL round-bottom flask (RBF) was charged with 4-methylpent-4-en-1-amine (338 mg, 2.0 mmol, 1.0 equiv), 2-nitro-1-(oxiran-2-ylmethyl)-1*H*-imidazole (396 mg, 4.0 mmol, 2.0 equiv), and EtOH (5 mL). The resulting mixture was heated to 50 °C and stirred overnight. The solvent was then removed in vacuo, and the crude reaction mixture was subjected to flash column chromatography (50% EtOAc/hexanes−5% MeOH/DCM) to afford product **1** as a yellow oil (54%). R_f = 0.16 (5% NEt_3, 50% EtOAc/hexane); ^{1}H NMR (500 MHz, CD_3OD): δ 7.45 (s, 1H), 7.12 (s, 1H), 4.47 (m, 2H), 4.66 (dd, J = 13.8, 3.6 Hz, 1H), 4.33 (dd, J = 13.8, 8.6 Hz, 1H), 4.07 (tt, J = 8.6, 3.6 Hz, 1H), 2.75 (dd, J = 12.2, 3.6 Hz, 1H), 2.64−2.61 (m, 3H), 2.07 (t, J = 7.5 Hz, 2H), 1.73 (s, 3H), 1.67 (p, J = 7.5 Hz, 2H); ^{13}C NMR (126 MHz, CD_3OD): δ 146.3, 129.2, 128.1, 113.2, 110.8, 69.5, 54.8, 53.4, 50.1, 36.3, 28.1, 22.4; FTIR (thin film): 2937, 1647, 1361, 1265 cm^{-1}; high resolution mass spectrometry-electrospray ionization (HRMS-ESI) (m/z) calcd for $C_{12}H_{21}N_4O_3$ ([M + H]$^+$): 269.1608; found: 269.1612.

*1-((2,2-Dimethylpent-4-en-1-yl)amino)-3-(2-nitro-1H-imidazol-1-yl)propan-2-ol (**3**).* A 50 mL RBF was charged with 2,2-dimethylpent-4-en-1-amine (676 mg, 4.0 mmol, 1.0 equiv), 2-nitro-1-(oxiran-2-ylmethyl)-1*H*-imidazole (904 mg, 8.0 mmol, 2.0 equiv), and EtOH (10 mL). The resulting mixture was heated to 60 °C and stirred overnight. The solvent was then removed in vacuo, affording **3** as an orange oil (98%). R_f = 0.14 (5% NEt_3, 50% EtOAc/hexane); ^{1}H NMR (500 MHz, $CDCl_3$): δ 7.16 (s, 1H), 6.87 (s, 1H), 5.65 (ddt, J = 16.1, 10.8, 7.5 Hz, 1H), 4.87 (d, J = 10.8 Hz, 1H), 4.86 (d, J = 16.1 Hz, 1H), 4.56 (dd, J = 13.8, 3.0 Hz, 1H), 4.15 (d, J = 13.8, 8.0 Hz, 1H), 3.94−3.91 (m, 1H), 2.64 (d, J = 12.2, 4.2 Hz, 1H), 2.43 (d, J = 12.2, 7.7 Hz, 1H), 2.27 (d, J = 11.5 Hz, 1H), 2.20 (d, J = 11.5 Hz, 1H), 1.86 (d, J = 7.5 Hz, 2H), 0.74 (s, 6H); ^{13}C NMR (126 MHz, $CDCl_3$): δ 144.4, 134.9, 127.7, 127.3, 116.8, 67.8, 59.8, 53.5, 52.7, 44.3, 34.1, 25.2; FTIR (thin film): 3334, 2958, 1639, 1488, 1361, 1162 cm^{-1}; HRMS-ESI (m/z) calcd for $C_{13}H_{23}N_4O_3$ ([M + H]$^+$): 283.1765; found: 238.1768.

*1-(5-Fluoro-3,3-dimethylpiperidin-1-yl)-3-(2-nitro-1H-imidazol-1-yl)propan-2-ol (**4**).* To a solution of **3** (141 mg, 0.5 mmol, 1.0 equiv) in *t*-BuOH (7.5 mL) was added NIS (113 mg, 0.5 mmol, 1.0 equiv) dissolved in *t*-BuOH (2.5 mL). The reaction was stirred at room temperature for 1.5 h. To the mixture was then added AgOTf (386 mg, 1.5 mmol, 3.0 equiv) and TBAF (1 M in tetrahydrofuran, THF, 1.5 mL, 1.5 mmol, 3.0 equiv). The resulting mixture was heated to 70 °C and stirred for 15 min. The reaction was cooled to room temperature, filtered through a plug of Celite, and the filtrate was concentrated in vacuo. The crude reaction mixture was purified by flash column chromatography (50% EtOAc/hexane−100% EtOAc) to afford **4** as a yellow solid (34%); R_f = 0.27 (5% NEt_3, 50% EtOAc/Hex); ^{1}H NMR (500 MHz, $CDCl_3$): δ 7.26 (s, 1H), 7.11 (s, 1H), 4.78−4.63 (m, 2H), 4.22 (ddd, J = 13.8, 10.1, 2.5 Hz, 1H), 4.12−4.04 (m, 1H), 2.86−2.72 (m, 1H), 2.53 (ddd, J = 12.4, 5.5, 4.0 Hz, 1H), 2.46−2.37 (m, 1H), 2.33−2.26 (m, 2H), 2.12−2.01 (m, 1H), 1.72−1.59 (m, 1H), 1.53−1.41 (m, 1H), 1.03 (s, 3H), 0.96 (s, 3H); ^{13}C NMR (126 MHz, $CDCl_3$): δ 144.9, 128.2, 127.7, 87.8 (d, J = 44.4 Hz), 86.4 (d, J = 43.6 Hz) 66.2, 60.3 (d, J = 15.4 Hz), 58.0 (d, J = 23.7 Hz), 53.5 (d, J = 11.8 Hz), 43.4 (d, J = 17.5 Hz), 31.8 (d, J = 34.3 Hz), 28.3 (d, J = 41.8 Hz), 27.3 (d, J = 60.3 Hz); FTIR (thin film): 3283, 3107, 2941, 1486, 1365 cm^{-1}; HRMS-ESI (m/z) calcd for $C_{13}H_{22}FN_4O_3$ ([M + H]$^+$): 301.1671; found: 301.1671.

*2,2-Dimethyl-N-(3-(2-nitro-1H-imidazol-1-yl)-2-((tetrahydro-2H-pyran-2-yl)oxy)propyl)pent-4-en-1-amine (**5**).* To a solution of 1-(3-azido-2-((tetrahydro-2*H*-pyran-2-yl)oxy)propyl)-2-nitro-1*H*-imidazole (148.1 mg, 0.5 mmol, 1.0 equiv) in dichloromethane (DCM) was added a solution of trimethylphosphine (1.0 M in toluene, 0.6 mL, 0.6 mmol, 1.2 equiv) under a N_2 atmosphere. The reaction was stirred at room temperature for 1.5 h; then, 2,2-dimethylpent-4-enal (112 mg, 1.0 mmol, 2.0 equiv) was added and stirred for 16 h. After that, $NaBH(OAc)_3$ (211.9 mg, 1.0 mmol, 2.0 equiv) was added at room temperature and stirred for 10 h. The reaction was quenched with saturated aqueous $NaHCO_3$ and extracted with DCM. Organic layers were concentrated in vacuo, and then subjected to flash column chromatography (100% EtOAc) to afford the product (55%). ^{1}H NMR (400 MHz, $CDCl_3$): δ 7.30 (s, 1H), 7.10 (s, 1H), 5.84−5.73 (m, 1H), 5.07-5.03 (m, 2H), 4.73-4.67 (m, 2H), 4.36 (s, 1H), 3.44−3.35 (m, 2H), 3.02 (m, 1H), 2.68 (dd, J = 12.6, 5.7 Hz, 1H), 2.54 (dd, J = 41.2, 11.7 Hz, 2H), 2.05 (d, J = 7.4 Hz, 2H), 1.72−1.70 (m, 1H), 1.55−1.39 (m, 6H), 0.96 (s, 6H). HRMS-ESI (m/z) calcd for $C_{18}H_{31}N_4O_4$ ([M + H]$^+$): 367.2345; found: 267.2340.

*5-Fluoro-3,3-dimethyl-1-(3-(2-nitro-1H-imidazol-1-yl)-2-((tetrahydro-2H-pyran-2-yl)oxy)propyl)piperidine (**6**).* To a solution of **5** (137 mg, 0.1 mmol, 1.0 equiv) in *t*-BuOH (0.5 mL) was added NIS (22.5 mg, 0.1 mmol, 1.0 equiv) dissolved in *t*-BuOH (0.5 mL). The reaction was stirred at room temperature for 1 h. To the mixture was then added AgOTf (76.8 mg, 0.3 mmol, 3.0 equiv) and TBAF (1 M in THF, 0.3 mL, 0.3 mmol, 3.0 equiv). The resulting mixture was heated to 70 °C and stirred for 1 h. The reaction was cooled to room temperature, filtered through a plug of Celite, and the filtrate was concentrated in vacuo. The crude reaction mixture was purified by flash column chromatography (50% EtOAc/Hexane−100% EtOAc) to afford **6** as a yellow solid (15%); R_f = 0.20 (10% MeOH/DCM); HRMS-ESI (m/z) calcd for $C_{18}H_{30}FN_4O_4$ ([M + H]$^+$): 385.2251; found: 385.2249.

*1-(3-(2-Nitro-1H-imidazol-1-yl)-2-((tetrahydro-2H-pyran-2-yl)-oxy)propyl)piperidin-4-yl 4-methylbenzenesulfonate (**7**).* ^{1}H NMR (400 MHz, $CDCl_3$): δ 7.78 (dd, J = 8.3, 2.2 Hz, 2H), 7.22 (d, J = 8.3 Hz, 2H), 7.22 (d, J = 1.1 Hz, 1H), 7.08 (d, J = 1.1 Hz, 1H), 4.79 (dd, J = 14.0, 3.2 Hz, 1H), 4.62 (dd, J = 4.8, 2.5 Hz, 1H), 4.53 (tt, J = 3.4, 11.1 Hz, 1H), 4.40 (dd, J = 14.0, 7.8 Hz, 1H), 4.09−4.18 (m, 1H), 3.25 (dd, J = 6.1, 4.0 Hz, 1H), 3.18 (dd, J = 7.3, 3.5 Hz, 1H), 2.55−2.63 (m, 3H), 2.44 (s, 3H), 2.26−2.32 (m, 5H), 1.37−1.47 (m, 8H).

Radiochemistry. The typical radiolabeling protocol for [^{18}F]-**20** to [^{18}F]-**22** is as follows: To the solution of ethane-1,2-diyl bis(4-methylbenzenesulfonate) (2 mg) in anhydrous acetonitrile (50 μL) within a cap-sealed v-vial, [^{18}F]-TBAF (216 mCi) in acetonitrile was added. The sealed reactor allows the reaction to be performed under pressure at 110 °C for 15 min. After diluting with 1.5 mL of solvent

https://doi.org/10.1021/acs.jmedchem.0c01962
J. Med. Chem. 2021, 64, 5593−5602

(water/acetonitrile: 2/3, v/v), the mixture was loaded to HPLC for purification. The HPLC method is described as follows: solvent A: 0.1% trifluoroacetic acid (TFA) water; solvent B: 0.1% TFA acetonitrile; and 0 to 2 min: isocratic elution of 40% solvent B, 2 to 22 min, 40−95% of solvent B. Flow rate: 3 mL/min. HPLC column: Gemini 5 μm C18 110 Å, 250 mm × 10.00 mm. [^{18}F]-2-fluoroethyl 4-methylbenzenesulfonate (77 mCi) was collected at 15 min. The collected [^{18}F]-2-fluoroethyl 4-methylbenzenesulfonate was diluted with 10 mL of water and then passed through a Sep-Pak tC18 cartridge. The loaded activity was washed out with 1 mL of acetonitrile. The elution was blow-dried in a v-vial, and then 20 μL of piperazine solution (0.33 μmol/mL) and 60 μL of acetonitrile were added and heated at 110 °C for a further 10 min. Then, K_2CO_3 (2 mg), 1-(2,3-epoxypropyl)-2-nitroimidazole (3.8 mg), and 60 μL of acetonitrile were added and heated at 90 °C for 20 min. The resulting tracer was purified by HPLC with the method described as follows: solvent A: 0.1% Et_3N water; solvent B: 0.1% Et_3N acetonitrile, 0 to 45 min: 5−30% of solvent B. Flow rate: 1 mL/min, collected at 17.6 min. RCY: 29.0%. [^{18}F]-**21** (0 to 35 min: 5−60% of solvent B. Flow rate: 1 mL/min, collected at 14.0 min. 22.8%) and [^{18}F]-**22** (0 to 35 min: 5−60% of solvent B. Flow rate: 1 mL/min, collected at 15.4 min, 28.8%) were synthesized accordingly using oxybis(ethane-2,1-diyl) bis(4-methylbenzenesulfonate) and homopiperazine as starting materials.

Typical Radiolabeling Protocol for [^{18}F]-23 to [^{18}F]-25. The precursor 2-(2-(vinylsulfonyl)ethoxy)ethyl 4-methylbenzenesulfonate (2 mg) was added into a v-vial and then the v-vial was sealed. Then, the [^{18}F]-TBAF (200 mCi) in acetonitrile was added and the vial was heated at 110 °C for 20 min. After diluting with 1 mL of water, the mixture was loaded to HPLC for purification. The HPLC method is described as follows: Solvent A: 0.1% TFA water; solvent B: 0.1% TFA acetonitrile; 0 to 2 min: isocratic elution of 5% solvent B, 2 to 22 min, 5−95% of solvent B. Flow rate: 3 mL/min. HPLC column: Gemini 5 μm C18 110 Å, 250 mm × 10.00 mm. [^{18}F]-((2-(2-fluoroethoxy)ethyl)sulfonyl)ethene (79 mCi) was collected at 13.6 min. Then, 2-nitroimidazole (2 mg) was mixed with the collected [^{18}F]-((2-(2-fluoroethoxy)ethyl)sulfonyl)ethene (5 mCi) in a solution of 50 μL of DMSO and 200 μL of 20× borate buffer (pH 8.5) and then heated at 80 °C for 20 min. The resulting tracer [^{18}F]-**23** was purified by HPLC with the method described as follows: 0 to 2 min: isocratic elution of 10% solvent B, 2 to 22 min, 10−55% of solvent B. Flow rate: 1 mL/min, collected at 12.4 min. RCY: 58.7%. [^{18}F]-**24** (12.4 min, 66.8%) and [^{18}F]-**25** (13.8 min, 53.1%) were synthesized accordingly using 4-nitroimidazole/[^{18}F]-((2-(2-fluoroethoxy)ethyl)sulfonyl)ethene and 2-nitroimidazole/[^{18}F]-((2-(2-(2-fluoroethoxy)ethoxy)ethyl)sulfonyl)ethene as starting materials.

Chemistry. *Synthesis of Precursor 2-(2-(2-(Vinylsulfonyl)-ethoxy)ethoxy)ethyl 4-Methylbenzenesulfonate (**18**).* The 2-(2-hydroxyethoxy)ethyl 4-methylbenzenesulfonate (384.9 mg, 1.0 equiv), which was synthesized according to the literature,[40] was stirred at room temperature with divinyl sulfone (262.0 mg, 1.5 equiv) and triphenylphosphine (39.3 mg, 0.1 equiv) in anhydrous dichloromethane (200 μL) for 2 h.[41] Then, the mixture was directly loaded on silica gel column chromatography for purification (ethyl acetate/hexane: 1/15—1/1). ^{1}H NMR (400 MHz, $CDCl_3$) δ 7.76 (d, J = 8.3 Hz, 2H), 7.33 (d, J = 8.1 Hz, 2H), 6.79-6.72 (m, 1H), 6.36 (d, J = 16.6 Hz, 1H), 6.08 (d, J = 9.9 Hz, 1H), 4.13−4.11 (m, 2H), 3.84 (t, J = 5.6 Hz, 2H), 3.65 (t, J = 4.8 Hz, 2H), 3.55 (s, 4H), 3.21 (t, J = 5.7 Hz, 2H), 2.42 (s, 3H). ^{13}C NMR (101 MHz, $CDCl_3$) δ 145.0, 137.9, 132.8, 129.9, 128.8, 127.9, 70.3, 69.2, 68.6, 64.6, 55.0. The precursor 2-(2-(vinylsulfonyl)ethoxy)ethyl 4-methylbenzenesulfonate (**16**) was synthesized accordingly with ethane-1,2-diol as the starting material. ^{1}H NMR (400 MHz, $CDCl_3$) δ 7.79 (d, J = 8.4 Hz, 2H), 7.36 (d, J = 8.1 Hz, 2H), 6.69 (m, 1H), 6.38 (d, J = 16.6 Hz, 1H), 6.07 (d, J = 9.9 Hz, 1H), 4.14 (m, 2H), 3.83 (t, J = 6.0 Hz, 2H), 3.65 (m, 2H), 3.19 (t, J = 5.6 Hz, 2H), 2.44 (s, 3H).^{13} C NMR (101 MHz, $CDCl_3$) δ 145.1, 137.7, 132.8, 129.9, 129.0, 127.9, 68.7, 68.7, 64.8, 54.8, 21.6.

Typical Procedure for the Synthesis of [^{19}F]-20. The *tert*-butyl 4-(2-fluoroethyl)piperazine-1-carboxylate (880 mg), which was prepared according to the literature method,[42] was dissolved in 2 mL of 50% v/v trifluoroacetic acid in dichloromethane. The reaction mixture was stirred at room temperature overnight and then evaporated under a vacuum to remove excess trifluoroacetic acid. Further purification was achieved by silica gel chromatography with ethyl acetate/methanol (10/1—2/1 v/v) as the eluent. 1-(2-fluoroethyl)piperazine: ^{1}H NMR (400 MHz, $CDCl_3$) δ 9.49 (s, 1H), 4.62 (t, J = 4.6 Hz, 1H), 4.50 (t, J = 4.7 Hz, 1H), 3.21 (t, J = 5.0 Hz, 4H), 2.83−2.79 (m, 5H), 2.73 (t, J = 4.7 Hz, 1H).

The mixture of 1-(2-fluoroethyl)piperazine (96.7 mg, 1.0 equiv), 2-nitro-1-(oxiran-2-ylmethyl)-1*H*-imidazole (85.8 mg, 1.3 equiv), and potassium carbonate (70.5 mg, 1.3 equiv) was mixed in 1 mL of acetonitrile and refluxed for 30 min, and then the mixture was cooled down to room temperature and stirred overnight. After purification using column chromatography with elution by ethyl acetate/methanol (10/1—2/1 v/v), the product was collected as an off-white solid.

*1-(4-(2-Fluoroethyl)piperazin-1-yl)-3-(2-nitro-1**H**-imidazol-1-yl)-propan-2-ol ([^{19}F]-**20**).* Off-white solid. ^{1}H NMR (400 MHz, $CDCl_3$) δ 7.26 (d, J = 0.9 Hz, 1H), 7.12 (d, J = 0.9 Hz, 1H), 4.70 (dd, J = 14.0, 2.5 Hz, 1H), 4.61 (t, J = 4.8 Hz, 1H), 4.49 (t, J = 4.8 Hz, 1H), 4.25 (dd, J = 14.0, 7.4 Hz, 1H), 4.05 (m, 1H), 2.73-2.45 (m, 12H), 2.28 (dd, J = 12.3, 10.2 Hz, 1H).^{13} C NMR (101 MHz, $CDCl_3$) δ 144.9, 128.0, 127.4, 82.7, 81.0, 65.7, 60.3, 58.1, 57.9, 53.4, 53.4, 53.3, 53.0. ^{19} F NMR (376 MHz, $CDCl_3$) δ −218.32. HRMS calcd for $C_{12}H_{21}FN_5O_3$ (M + H), 302.1628; found, 302.1630.

Typical Procedure for the Syntheses of Standards [^{19}F]-21 and [^{19}F]-22. 1-(4-(2-(2-fluoroethoxy)ethyl)piperazin-1-yl)-3-(2-nitro-1*H*-imidazol-1-yl)propan-2-ol (**21**): Off-white solid. ^{1}H NMR (400 MHz, $CDCl_3$) δ 7.25 (d, J = 0.9 Hz, 1H), 7.11 (d, J = 0.9 Hz, 1H), 4.68 (dd, J = 14.0 Hz, 1H), 4.58 (t, J = 4.1 Hz, 1H), 4.47 (t, J = 4.1 Hz, 1H), 4.23 (dd, J = 14.0, 7.4 Hz, 1H), 4.02 (m, 1H), 3.71 (t, J = 4.2 Hz, 1H), 3.64-3.60 (m, 3H), 2.65-2.63 (m, 2H), 2.58 (t, J = 5.8 Hz, 2H), 2.51-2.42 (m, 7H), 2.25 (dd, J = 12.2, 10.2 Hz, 1H). ^{13} C NMR (101 MHz, $CDCl_3$) δ 144. 9, 128.0, 127.4, 83.9, 82.3, 70.3, 70.1, 69.1, 65.6, 60.3, 57.6, 53.5, 53.3. ^{19} F NMR (376 MHz, $CDCl_3$) δ −222.72. HRMS calcd for $C_{14}H_{25}FN_5O_4$ (M + H), 346.1891; found, 346.1892.

*1-(4-(2-Fluoroethyl)-1,4-diazepan-1-yl)-3-(2-nitro-1H-imidazol-1-yl)propan-2-ol ([^{19}F]-**22**).* Off-white solid. ^{1}H NMR (400 MHz, $CDCl_3$) δ 7.28 (d, J = 0.9 Hz, 1H), 7.12 (d, J = 0.9 Hz, 1H), 4.69 (dd, J = 13.9, 2.4 Hz, 1H), 4.57 (t, J = 5.0 Hz, 1H), 4.45 (t, J = 5.2 Hz, 1H), 4.22 (dd, J = 13.9, 7.6 Hz, 1H), 3.96 (m, 1H), 2.88-2.67 (m, 11H), 2.29 (dd, J = 12.4, 10.4 Hz, 1H), 1.80 (m, 2H). ^{13} C NMR (101 MHz, $CDCl_3$) δ 142.8, 128.1, 127.4, 83.2, 81.6, 66.4, 60.4, 57.9, 57.7, 55.6, 55.6, 55.4, 54.5, 54.3, 54.3, 53.3, 28.0. ^{19} F NMR (376 MHz, $CDCl_3$) δ −219.37. HRMS calcd for $C_{13}H_{23}FN_5O_3$ (M + H), 316.1785; found, 316.1791.

Typical Procedure for the Synthesis of [^{19}F]-23. To the solution of 2-fluoroethanol (64.1 mg, 1.0 equiv) and divinyl sulfone (177.2 mg, 1.5 equiv) in anhydrous dichloromethane (200 μL), triphenylphosphine (26.2 mg, 0.1 equiv) was added as portion.[28] The mixture was stirred at room temperature for 2 h and then directly loaded on silica gel column chromatography for purification (ethyl acetate/hexane 1/20−1/5). (2-(2-fluoroethoxy)ethylsulfonyl)ethane (51.2 mg, 1.0 equiv) and 2-nitroimidazole (63.5 mg, 2.0 equiv) were mixed in a solution of 200 μL of DMSO and 500 μL of 20× borate buffer (pH 8.5) and then heated at 80 °C for 2 h; 5 mL of water and 5 mL of ethyl acetate were added to the reaction mixture. After extracting the aqueous phase three times, the organic solutions were combined and dried over anhydrous $MgSO_4$. The solvent was evaporated under reduced pressure, and the residue was purified by elution with ethyl acetate/hexane (1/5—2/1) to get the product as an off-white solid.

*1-(2-((2-(2-fluoroethoxy)ethyl)sulfonyl)ethyl)-2-nitro-1**H**-imidazole ([^{19}F]-**23**).* Off-white solid. ^{1}H NMR (400 MHz, acetone-d_6) δ 7.58 (d, J = 0.9 Hz, 1H), 7.14 (d, J = 0.9 Hz, 1H), 4.98 (t, J = 6.7 Hz, 2H), 4.62 (t, J = 4.0 Hz, 1H), 4.50 (t, J = 4.0 Hz, 1H), 3.93 (t, J = 5.3 Hz, 2H), 3.82 (t, J = 6.7 Hz, 2H), 3.79 (d, J = 4.0 Hz, 1H), 3.71 (t, J = 4.0 Hz, 1H), 3.31 (t, J = 5.4 Hz, 2H). ^{13} C NMR (101 MHz, acetone-d_6) δ 128.6, 128.5, 84.4, 82.8, 71.2, 71.0, 65. 5, 54.9, 54.8, 44.1. ^{19} F NMR (376 MHz, acetone-d_6) δ −223.39. HRMS calcd for $C_9H_{15}FN_3O_5S$ (M + H), 296.0716; found, 296.0712.

https://doi.org/10.1021/acs.jmedchem.0c01962
J. Med. Chem. 2021, 64, 5593−5602

The syntheses of standards for [^{19}F]-**24** and [^{19}F]-**25** were according to the typical procedure.

1-(2-((2-(2-fluoroethoxy)ethyl)sulfonyl)ethyl)-4-nitro-1*H*-imidazole ([^{19}F]-**24**) was obtained as an off-white solid. ^{1}H NMR (400 MHz, acetone-d_6) δ 8.26 (d, J = 1.5 Hz, 1H), 7.80 (d, J = 1.4 Hz, 1H), 4.72 (t, J = 6.8 Hz, 2H), 4.65 (t, J = 4.0 Hz, 1H), 5.53 (t, J = 4.0 Hz, 1H), 3.95 (t, J = 5.2 Hz, 2H), 3.83 (t, J = 6.8 Hz, 2H), 3.80 (d, J = 8.0 Hz, 1H), 3.74 (t, J = 4.0 Hz, 1H), 3.38 (t, J = 5.4 Hz, 1H). ^{13}C NMR (101 MHz, acetone-d_6) δ 137.2, 137.2, 120.7, 83.6, 81.9, 70.3, 70.1, 64.7, 54.3, 54.0, 41.2. ^{19}F NMR (376 MHz, acetone-d_6) δ −223.35. HRMS calcd for $C_9H_{15}FN_3O_5S$ (M + H), 296.0716; found, 296.0708.

1-(2-((2-(2-(2-Fluoroethoxy)ethoxy)ethyl)sulfonyl)ethyl)-2-nitro-1*H*-imidazole ([^{19}F]-**25**) was obtained as a white solid. ^{1}H NMR (400 MHz, acetone-d_6) δ 7.59 (s, 1H), 7.13 (s, 1H), 4.97 (t, J = 6.6 Hz, 2H), 4.56 (t, J = 4.0 Hz, 1H), 4.44 (t, J = 4.0 Hz, 1H), 3.89 (t, J = 5.2 Hz, 2H), 3.84 (t, J = 6.6 Hz, 2H), 3.72 (t, J = 4.1 Hz, 1H), 3.66-3.64 (m, 5H), 3.28 (t, J = 5.3 Hz, 2H). ^{13}C NMR (101 MHz, acetone-d_6) δ 127.7, 127.6, 83.8, 82.2, 70.2, 70.1, 70.0, 69.9, 64.6, 54.0, 53.9, 43.4. ^{19}F NMR (376 MHz, acetone-d_6) δ −223.35. HRMS calcd for $C_{11}H_{19}FN_3O_6S$ (M + H), 340.0979; found, 340.0966.

The synthesis of [^{18}F]-FMISO was modified from the literature.[43] The 1-(2′-nitro-1′-imidazolyl)-2-*O*-tetra-hydropyranyl-3-*O*-toluenesulfonyl propanediol (NITTP, 2 mg) precursor was heated with 247 mCi of [^{18}F]-TBAF in acetonitrile at 110 °C for 10 min. After removing the solvent by blow-drying, 1 mL of 1 N HCl was added to the reaction mixture and heated at 105 °C for 5 min. The mixture was cooled down to room temperature, and 0.5 mL of 2 N NaOH was added to neutralize the reaction mixture. After passing the mixture through a Sep-Pak alumina N cartridge, the activity was loaded on HPLC (isocratic ethanol/water 5/95). [^{18}F]-FMISO (145 mCi) was collected at 13.5 min after separation.

2-(2-((2-(2-nitro-1*H*-imidazol-1-yl)ethyl)sulfonyl)ethoxy)ethyl 4-methylbenzenesulfonate (**26**) was synthesized with 2-(2-(vinylsulfonyl)ethoxy)ethyl 4-methylbenzenesulfonate and 2-nitroimidazole as starting materials in borate buffer. ^{1}H NMR (400 MHz, acetone-d_6) δ 7.81 (d, J = 8.3 Hz, 2H), 7.58 (d, J = 1.0 Hz, 1H), 7.49 (d, J = 8.0 Hz, 2H), 7.13 (d, J = 1.0 Hz, 1H), 4.94 (t, J = 6.7 Hz, 2H), 4.23 (t, J = 4.4 Hz, 2H), 3.86 (t, J = 5.2 Hz, 2H), 3.78-3.72 (m, 4H), 3.30 (t, J = 5.4 Hz, 2H), 2.45 (s, 3H). ^{13}C NMR (101 MHz, acetone-d_6) δ 145.1, 133.3, 130.0, 127.8, 127.8, 127.8, 127.6, 69.3, 68.6, 64.6, 53.9, 53.8, 43.1, 20.6. HRMS calcd for $C_{16}H_{22}N_3O_8S_2$ (M + H), 448.0848; found, 448.0820.

Mouse Models. All animal studies were reviewed and approved by the University of North Carolina at the Chapel Hill Institutional Animal Care and Use Committee. The FaDu tumor cell was obtained from the LCCC tissue culture facility (University of North Carolina at Chapel Hill, Chapel Hill, NC). The UPPL tumor cell was a gift from Prof. Kim's group. The FaDu tumor-bearing nude mice and UPPL tumor-bearing C57BL/6 mice were established according to the literature method.[44,45]

Small-Animal PET. FaDu tumor- or UPPL tumor-bearing mice were intravenously injected via the tail vein with an [^{18}F]-tracer (three mice in a group). The animals were fresh and only injected once for PET imaging. For FaDu tumor-bearing mice (injection dose: 6.0−8.9 μCi/g), a 10 min static emission scan was acquired with a SuperArgus small-animal PET/CT scanner at 30 min and 120 min postinjection. For UPPL tumor-bearing mice (injection dose: 5.0−9.1 μCi/g), a 10 min static emission scan was acquired at 30 min, 1, 2, and 4 h pi The regions of interest (ROIs) were drawn over the tumor and other organs and calculated as %ID/g. The mean uptake and standard deviation (mean ± SD) were calculated for each group, and the number of organs we tested in each group was calculated as the n value.

***In Vitro* Stability.** The *in vitro* stability study was determined on an Agilent HPLC. In brief, [^{18}F]-**23** (238 μCi) was incubated with 400 μL of plasma at 37 °C for 0.5, 1, and 2 h. After the serum protein was precipitated and centrifuged, the liquid supernatant was then analyzed by radio-HPLC.

***In Vivo* Stability.** The *in vivo* stability study was determined using normal mice. In brief, [^{18}F]-**23** (207−213 μCi) was injected into the animal, and blood samples were collected at 0.5, 1, and 2 h pi. After the blood protein was precipitated and centrifuged, the liquid supernatant was then analyzed by radio-HPLC or γ counting.

Pimonidazole Staining and Autoradiography Study. Pimonidazole was injected intravenous (iv) at around 120 min before euthanasia, followed by an [^{18}F]-**23** injection. After PET imaging with [^{18}F]-**23**, the tumors were collected and 10 μm thin tissue sections were obtained from the frozen tumor blocks using a cryostat with an optimal cutting temperature compound. For cutting, four slices were obtained at each location with two sections mounted on each slice. Odd number slices were used for autoradiography and even number ones were used for pimonidazole fluorescence staining. Then, about 15−20 sections were skipped and the tumor sections were collected as described above until the whole tumor was cut. Thereafter, these fresh-frozen sections were dried. Autoradiography studies were performed using the Cyclone Plus storage phosphor system (Perkin Elmer), and all phosphor images in these studies had a 25 μm pixel resolution. For pimonidazole staining of the neighboring slices, the sections were fixed with acetone for 10 min, washed twice in phosphate-buffered saline (PBS) (5 min each), and immersed in 0.3% Tween-20 for 20 min at RT. Then, the slices were blocked in primary AB dilution buffer (Biomeda, Foster City) for 30 min to block nonspecific binding and incubated with mouse anti-pimonidazole Mab HP7-DyLight549 (1:500 in PBS) in the dark for 1 h at RT. After washing with PBS three times (5 min each), the slices were covered with EverBrite mounting medium containing 4,6-diamino-2-phenylindole (DAPI, Biotium, CA) and observed under a Zeiss LSM 710 laser scanning microscope (Zeiss, Jena, German).

■ ASSOCIATED CONTENT

Supporting Information

The Supporting Information is available free of charge at https://pubs.acs.org/doi/10.1021/acs.jmedchem.0c01962.

Molecular strings (CSV)

Additional figures illustrating HPLC data, experimental details, molecular formula strings, and NMR spectra (PDF)

■ AUTHOR INFORMATION

Corresponding Authors

Zhanhong Wu − *Biomedical Research Imaging Center, Department of Radiology, and UNC Lineberger Comprehensive Cancer Center, University of North Carolina-Chapel Hill, Chapel Hill, North Carolina 27514, United States*; Email: zhhwu@med.unc.edu

Qiu Wang − *Department of Chemistry, Duke University, Durham, North Carolina 27708, United States*; orcid.org/0000-0002-6803-9556; Email: qiu.wang@duke.edu

Authors

Li Wang − *Biomedical Research Imaging Center, Department of Radiology, and UNC Lineberger Comprehensive Cancer Center, University of North Carolina-Chapel Hill, Chapel Hill, North Carolina 27514, United States; Department of Nuclear Medicine, Affiliated Hospital of Southwest Medical University, Luzhou 646000, China; Nuclear Medicine and Molecular Imaging Key Laboratory of Sichuan Province, Luzhou 646000, Sichuan, China*

Hui Wang − *Biomedical Research Imaging Center, Department of Radiology, and UNC Lineberger Comprehensive Cancer Center, University of North Carolina-Chapel Hill, Chapel Hill, North Carolina 27514, United States*

https://doi.org/10.1021/acs.jmedchem.0c01962
J. Med. Chem. 2021, 64, 5593−5602

Kun Shen − *Department of Chemistry, Duke University, Durham, North Carolina 27708, United States*
Hyejin Park − *Department of Chemistry, Duke University, Durham, North Carolina 27708, United States*
Tao Zhang − *Biomedical Research Imaging Center, Department of Radiology, and UNC Lineberger Comprehensive Cancer Center, University of North Carolina-Chapel Hill, Chapel Hill, North Carolina 27514, United States*
Xuedan Wu − *Biomedical Research Imaging Center, Department of Radiology, and UNC Lineberger Comprehensive Cancer Center, University of North Carolina-Chapel Hill, Chapel Hill, North Carolina 27514, United States;* orcid.org/0000-0001-5875-4233
Mei Hu − *Department of Nuclear Medicine, Affiliated Hospital of Southwest Medical University, Luzhou 646000, China; Nuclear Medicine and Molecular Imaging Key Laboratory of Sichuan Province, Luzhou 646000, Sichuan, China*
Hong Yuan − *Biomedical Research Imaging Center, Department of Radiology, and UNC Lineberger Comprehensive Cancer Center, University of North Carolina-Chapel Hill, Chapel Hill, North Carolina 27514, United States*
Yue Chen − *Department of Nuclear Medicine, Affiliated Hospital of Southwest Medical University, Luzhou 646000, China; Nuclear Medicine and Molecular Imaging Key Laboratory of Sichuan Province, Luzhou 646000, Sichuan, China*
Zibo Li − *Biomedical Research Imaging Center, Department of Radiology, and UNC Lineberger Comprehensive Cancer Center, University of North Carolina-Chapel Hill, Chapel Hill, North Carolina 27514, United States;* orcid.org/0000-0002-1063-0298

Complete contact information is available at: https://pubs.acs.org/10.1021/acs.jmedchem.0c01962

Author Contributions

This manuscript was written through contributions of all authors. All authors have given approval to the final version of the manuscript.

Funding

The research was partially supported by the UNC Department of Radiology, the Biomedical Research Imaging Center, and the UNC Lineberger Comprehensive Cancer Center (start-up fund to Z.W.), the National Institutes of Health (5R01CA233904, 1R01EB029451, and 1S10OD023611) (Z.L.), the National Science Foundation (CHE-1455220) and the Camille and Henry Dreyfus Foundation (Q.W.).

Notes

The authors declare no competing financial interest.

■ ACKNOWLEDGMENTS

The authors are grateful to Prof. William Kim for providing UPPL cancer cells and Dr. Gerald T. Bida for excellent technical support on cyclotron operation.

■ ABBREVIATIONS

NIS, *N*-iodosuccinimide; THP, 2-tetrahydropyranyl; TLC, thin-layer chromatography; RT, room temperature; TBAF, tetra-*n*-butylammonium fluoride; PEG, poly(ethylene glycol); RCY, radiochemistry yield

■ REFERENCES

(1) Ali, I.; Lone, M. N.; Aboul-Enein, H. Y. Imidazoles as potential anticancer agents. *Med. Chem. Commun.* **2017**, *8*, 1742−1773.
(2) Ren, Y.; de Blanco, E. J. C.; Fuchs, J. R.; Soejarto, D. D.; Burdette, J. E.; Swanson, S. M.; Kinghorn, A. D. Potential anticancer agents characterized from selected tropical plants. *J. Nat. Prod.* **2019**, *82*, 657−679.
(3) Saleem, K.; Wani, W. A.; Haque, A.; Lone, M. N.; Hsieh, M.; Jairajpuri, M. A.; Ali, I. Synthesis, DNA binding, hemolysis assays and anticancer studies of copper (II), nickel (II) and iron (III) complexes of a pyrazoline-based ligand. *Future Med. Chem.* **2013**, *5*, 135−146.
(4) Ali, I.; Saleem, K.; Wesselinova, D.; Haque, A. Synthesis, DNA binding, hemolytic, and anti-cancer assays of curcumin I-based ligands and their ruthenium (III) complexes. *Med. Chem. Res.* **2013**, *22*, 1386−1398.
(5) Ali, I.; Wani, W. A.; Saleem, K.; Hseih, M. Design and synthesis of thalidomide based dithiocarbamate Cu (II), Ni (II) and Ru (III) complexes as anticancer agents. *Polyhedron* **2013**, *56*, 134−143.
(6) Scott, A. M.; Wolchok, J. D.; Old, L. J. Antibody therapy of cancer. *Nat. Rev. Cancer* **2012**, *12*, 278−287.
(7) Park, S.; Nam, J. The force awakens: metastatic dormant cancer cells. *Exp. Mol. Med.* **2020**, *52*, 569−581.
(8) Wilson, W. R.; Hay, M. P. Targeting hypoxia in cancer therapy. *Nat. Rev. Cancer* **2011**, *11*, 393−410.
(9) Horsman, M. R.; Mortensen, L. S.; Petersen, J. B.; Busk, M.; Overgaard, J. Imaging hypoxia to improve radiotherapy outcome. *Nat. Rev. Clin. Oncol.* **2012**, *9*, 674−687.
(10) Harris, A. L. Hypoxia–a key regulatory factor in tumour growth. *Nat. Rev. Cancer* **2002**, *2*, 38−47.
(11) Milosevic, M.; Warde, P.; Ménard, C.; Chung, P.; Toi, A.; Ishkanian, A.; McLean, M.; Pintilie, M.; Sykes, J.; Gospodarowicz, M.; Catton, C.; Hill, R. P.; Bristow, R. Tumor hypoxia predicts biochemical failure following radiotherapy for clinically localized prostate cancer. *Clin. Cancer Res.* **2012**, *18*, 2108−2114.
(12) Nordsmark, M.; Loncaster, J.; Aquino-Parsons, C.; Chou, S. C.; Ladekarl, M.; Havsteen, H.; Lindegaard, J. C.; Davidson, S. E.; Varia, M.; West, C.; Hunter, R.; Overgaard, J.; Raleigh, J. A. Measurements of hypoxia using pimonidazole and polarographic oxygen-sensitive electrodes in human cervix carcinomas. *Radiother. Oncol.* **2003**, *67*, 35−44.
(13) Bussink, J.; Kaanders, J. H.A.M.; van der Kogel, A. J. Tumor hypoxia at the micro-regional level: clinical relevance and predictive value of exogenous and endogenous hypoxic cell markers. *Radiother. Oncol.* **2003**, *67*, 3−15.
(14) Brinkhuizen, T.; Weijzen, C. A.; Eben, J.; Thissen, M. R.; van Marion, A. M.; Lohman, B. G.; Winnepenninckx, V. J.; Nelemans, P. J.; van Steensel, M. A. Immunohistochemical analysis of the mechanistic target of rapamycin and hypoxia signalingpathways in basal cell carcinoma and trichoepithelioma. *PLoS One* **2014**, *9*, No. e106427.
(15) Fan, Q.; Tang, C. Y.; Gu, D.; Zhu, J.; Li, G.; Wu, Y.; Tao, X. Investigation of hypoxia conditions using oxygen-enhanced magnetic resonance imaging measurements in glioma models. *Oncotarget* **2017**, *8*, 31864−31875.
(16) Verwer, E. E.; Boellaard, R.; van der Veldt, A. Positron emission tomography to assess hypoxia and perfusion in lung cancer. *World J. Clin. Oncol.* **2014**, *5*, 824−844.
(17) Lopci, E.; Grassi, I.; Chiti, A.; Nanni, C.; Cicoria, G.; Toschi, L.; Fonti, C.; Lodi, F.; Mattioli, S.; Fanti, S. PET radiopharmaceuticals for imaging of tumor hypoxia: a review of the evidence. *Am. J. Nucl. Med. Mol. Imaging* **2014**, *4*, 365−384.
(18) Stieb, S.; Eleftheriou, A.; Warnock, G.; Guckenberger, M.; Riesterer, O. Longitudinal PET imaging of tumor hypoxia during the course of radiotherapy. *Eur. J. Nucl. Med. Mol. Imaging* **2018**, *45*, 2201−2217.
(19) Tong, X.; Srivatsan, A.; Jacobson, O.; Wang, Y.; Wang, Z.; Yang, X.; Niu, G.; Kiesewetter, D. O.; Zheng, H.; Chen, X. Monitoring tumor hypoxia using (18)F-FMISO PET and pharmaco-

kinetics modeling after photodynamic therapy. *Sci. Rep.* **2016**, *6*, No. 31551.
(20) Verwer, E. E.; Bahce, I.; van Velden, F. H.; Yaqub, M.; Schuit, R. C.; Windhorst, A. D.; Raijmakers, P.; Hoekstra, O. S.; Lammertsma, A. A.; Smit, E. F.; Boellaard, R. Parametric methods for quantification of 18F-FAZA kinetics in non-small cell lung cancer patients. *J. Nucl. Med.* **2014**, *55*, 1772−1777.
(21) Hoigebazar, L.; Jeong, J. M.; Hong, M. K.; Kim, Y. J.; Lee, J. Y.; Shetty, D.; Lee, Y. S.; Lee, D. S.; Chung, J. K.; Lee, M. C. Synthesis of 68Ga-labeled DOTA-nitroimidazole derivatives and their feasibilities as hypoxia imaging PET tracers. *Bioorg. Med. Chem.* **2011**, *19*, 2176−2181.
(22) ClinicalTrials.gov Identifier: NCT03573986.
(23) ClinicalTrials.gov Identifier: NCT01542177.
(24) Busk, M.; Jakobsen, S.; Horsman, M. R.; Mortensen, L. S.; Iversen, A. B.; Overgaard, J.; Nordsmark, M.; Ji, X.; Lee, D. Y.; Raleigh, J. R. PET imaging of tumor hypoxia using 18F-labeled pimonidazole. *Acta Oncologica* **2013**, *52*, 1300−1307.
(25) Ortiz, G. X., Jr.; Chansaenpak, K.; Wang, M.; Ma, X.; Wang, H.; Li, Z.; Wang, Q. A novel ^{18}F-labeling method for the synthesis of [^{18}F]-piperidine-containing ligands as potential PET radiotracers for σ receptors. *Synlett* **2018**, *29*, 410−414.
(26) Erlandsson, M.; Karimi, F.; Takahashi, K.; Långström, B. ^{18}F-Labelled vorozole analogues as PET tracer for aromatase. *J. Labelled Compd. Radiopharm.* **2008**, *51*, 207−212.
(27) Perruchon, J.; Ortmann, R.; Altenkämper, M.; Silber, K.; Wiesner, J.; Jomaa, H.; Klebe, G.; Schlitzer, M. Studies addressing the importance of charge in the binding of fosmidomycin-like molecules to deoxyxylulosephosphate reducto isomerase. *ChemMedChem* **2008**, *3*, 1232−1241.
(28) Kapadnis, P. B.; Hall, E.; Ramstedt, M.; Galloway, W. R.; Welch, M.; Spring, D. R. Towards quorum-quenching catalytic antibodies. *Chem. Commun.* **2009**, *5*, 538−540.
(29) Fairlamb, I. J.; Dickinson, J. M.; O'Connor; Cohen, L. H.; van Thiel, C. F. Synthesis and antimicrobial evaluation of farnesyl diphosphate mimetics. *Bioorg. Chem.* **2003**, *31*, 80−97.
(30) Morales-Sanfrutos, J.; Lopez-Jaramillo, J.; Ortega-Muñoz, M.; Megia-Fernandez, A.; Perez-Balderas, F.; Hernandez-Mateo, F.; Santoyo-Gonzalez, F. Vinyl sulfone: a versatile function for simple bioconjugation and immobilization. *Org. Biomol. Chem.* **2010**, *8*, 667−675.
(31) Wu, Z.; Li, L.; Liu, S.; Yakushijin, F.; Yakushijin, K.; Horne, D.; Conti, P. S.; Li, Z.; Kandeel, F.; Shively, J. E. Facile preparation of a thiol-reactive ^{18}F-labeling agent and synthesis of ^{18}F-DEG-VS-NT for PET imaging of a neurotensin receptor−positive tumor. *J. Nucl. Med.* **2014**, *55*, 1178−1184.
(32) Li, L.; Tsai, S. W.; Anderson, A. L.; Keire, D. A.; Raubitschek, A. A.; Shively, J. E. Vinyl sulfone bifunctional derivatives of DOTA allow sulfhydryl- or amino-directed coupling to antibodies. Conjugates retain immunoreactivity and have similar biodistributions. *Bioconjugate Chem.* **2002**, *13*, 110−115.
(33) McCall, K. C.; Humm, J. L.; Bartlett, R.; Reese, M.; Carlin, S. Copper-64-diacetyl-bis(N(4)-methylthiosemicarbazone) pharmacokinetics in FaDu xenograft tumors and correlation with microscopic markers of hypoxia. *Int. J. Radiat. Oncol. Biol. Phys.* **2012**, *84*, 393−399.
(34) Xue, M.; Chen, W.; Xiang, A.; Wang, R.; Chen, H.; Pan, J.; Pang, H.; An, H.; Wang, X.; Hou, H.; Li, X. Hypoxic exosomes facilitate bladder tumor growth and development through transferring longnon-coding RNA-UCA1. *Mol. Cancer* **2017**, *16*, 143−155.
(35) Ord, J. J.; Streeter, E. H.; Roberts, I. S.; Cranston, D.; Harris, A. L. Comparison of hypoxia transcriptome *in vitro* with *in vivo* gene expression in human bladder cancer. *Br. J. Cancer* **2005**, *93*, 346−354.
(36) Saito, R.; Smith, C. C.; Utsumi, T.; Bixby, L. M.; Kardos, J.; Wobker, S. E.; Stewart, K. G.; Chai, S.; Manocha, U.; Byrd, K. M.; Damrauer, J. S.; Williams, S. E.; Vincent, B. G.; Kim, W. Y. Molecular subtype-specific immunocompetent models of high-grade urothelial carcinoma reveal differential neoantigen expression and response to immunotherapy. *Cancer Res.* **2018**, *78*, 3954−3968.
(37) Dubois, L.; Landuyt, W.; Haustermans, K.; Dupont, P.; Bormans, G.; Vermaelen, P.; Flamen, P.; Verbeken, E.; Mortelmans, L. Evaluation of hypoxia in an experimental rat tumor model by [(18)F]fluoromisonidazole PET and immunohistochemistry. *Br. J. Cancer* **2004**, *91*, 1947−1954.
(38) Troost, E. G.; Laverman, P.; Philippens, M. E.; Lok, J.; van der Kogel, A. J.; Oyen, W. J.; Boerman, O. C.; Kaanders, J. H.; Bussink, J. Correlation of [18F]FMISO autoradiography and pimonidazole [corrected] immunohistochemistry in human head and neck carcinoma xenografts. *Eur. J. Nucl. Med. Mol. Imaging* **2008**, *35*, 1803−1811.
(39) Busk, M.; Mortensen, L. S.; Nordsmark, M.; Overgaard, J.; Jakobsen, S.; Hansen, K. V.; Theil, J.; Kallehauge, J. F.; D'Andrea, F. P.; Steiniche, T.; Horsman, M. R. PET hypoxia imaging with FAZA: reproducibility at baseline and during fractionated radiotherapy in tumor-bearing mice. *Eur. J. Nucl. Med. Mol. Imaging* **2013**, *40*, 186−197.
(40) Davis, O. A.; Bull, J. A. Synthesis of di-, tri-, and tetrasubstituted oxetanes by rhodium-catalyzed O-H insertion and C-C bond-forming cyclization. *Angew. Chem., Int. Ed.* **2014**, *53*, 14230−14234.
(41) Strasser, S.; Slugovc, C. Nucleophile-mediated oxa-Michael addition reactions of divinylsulfone−a thiol-free option for step-growth polymerizations. *Catal. Sci. Technol.* **2015**, *5*, 5091−5094.
(42) Breyholz, H. J.; Wagner, S.; Faust, A.; Riemann, B.; Höltke, C.; Hermann, S.; Schober, O.; Schäfers, M.; Kopka, K. Radiofluorinated pyrimidine-2,4,6-triones as molecular probes for noninvasive MMP-targeted imaging. *ChemMedChem.* **2010**, *5*, 777−789.
(43) Tang, G.; Wang, M.; Tang, X.; Gan, M.; Luo, L. Fully automated one-pot synthesis of [^{18}F]fluoromisonidazole. *Nucl. Med. Biol.* **2005**, *32*, 553−558.
(44) Li, F.; Jørgensen, J. T.; Forman, J.; Hansen, A. E.; Kjaer, A. ^{64}Cu-ATSM reflects pO_2 levels in human head and neck cancer xenografts but not in colorectal cancer xenografts: Comparison with $^{64}CuCl_2$. *J. Nucl. Med.* **2016**, *57*, 437−443.
(45) Jiang, W.; Yin, L.; Chen, H.; Paschall, A. V.; Zhang, L.; Fu, W.; Zhang, W.; Todd, T.; Yu, K. S.; Zhou, S.; Zhen, Z.; Butler, M.; Yao, L.; Zhang, F.; Shen, Y.; Li, Z.; Yin, A.; Yin, H.; Wang, X.; Avci, F. Y.; Yu, X.; Xie, J. NaCl nanoparticles as a cancer therapeutic. *Adv. Mater.* **2019**, *31*, No. e1904058.

https://doi.org/10.1021/acs.jmedchem.0c01962
J. Med. Chem. 2021, 64, 5593−5602